Mathematical modeling and numerical simulations of reactive flows in channels

F. Platte*, O. Mierka, S. Hysing, M. N. Kashid, and S. Turek

Institute of Applied Mathematics (LS III), University of Dortmund
Vogelpothsweg 87, D-44227, Dortmund, Germany

Abstract

The macroscopic behavior of a chemical process is essentially driven by kinetic phenomena. For most chemical processes one has to deal with more or less complex flows which define the mixing quality and/or mass transfer. Chemical reactions in these types of systems to a large extent depend on the underlying flow patterns. In this paper we present a short review on mathematical modeling and numerical simulations of different types of chemical processes. The appropriate mathematical description of the flow and the correct implementation of reactions for three different cases of gas-solid, single-phase liquid, and liquid-liquid flow in a channel are presented. Finally the obtained results are compared with experimental data.

Key Words: single-phase flow, two-phase flow, chemical reaction, mixing, mass-transfer

1 Introduction

In recent years more and more efforts are being made to combine fluid flow models with conventional reaction engineering models. Due to relatively new developments in the field of computational fluid dynamics (CFD) there is comparatively little information available concerning the detailed modeling and simulation of complex chemical processes. For any such process the starting point is the mass, momentum (here by the Navier-Stokes equations), and heat balances

$$\frac{\partial(\rho V)}{\partial t} + \mathbf{u} \cdot \nabla(\rho V) = \varphi \tag{1}$$

$$\frac{\partial \mathbf{u}}{\partial t} + \mathbf{u} \cdot \nabla \mathbf{u} - \nu \Delta \mathbf{u} = -\nabla p + \mathbf{f} \tag{2}$$

$$\frac{\partial T}{\partial t} + \mathbf{u} \cdot \nabla T - \alpha \Delta T = Q. \tag{3}$$

The above set of equations can be simplified for a given process depending on the change in density (incompressibility or compressibility), velocity (stationary or non-stationary), and temperature (isothermal or non-isothermal).

If the velocity changes are not significant in a given chemical process the momentum balance is usually not considered in order to reduce to computational effort. One such example is Poiseuille flow in channels where the flow patterns are well-defined and the velocity is therefore considered to be constant. As a result the mathematical model for these types of problems reduces to a coupled set of heat and mass balances. Though the flow field is relatively simple (laminar, stationary, and single-phase), a rather complex behavior can sometimes be found due to the interaction of mass transfer, sorption, and nonlinear

*Correspondence to: fplatte@math.uni-dortmund.de

reactions. Additional complexity might result from dynamic operating conditions, e.g. periodic flow reversal or combined reactive/regenerative processes.

Chemical engineering processes are often realized in turbulent flow conditions due to the higher efficiency of the desired mixing phenomenon. The role of mixing is especially crucial when it becomes the limiting step of a process. A tycical example is a process involving fast chemical reactions. In this case the introduced feed streams of pure chemical species have to be premixed on the microscale level in order to enable the reaction to take place. This way, the process is being limited by the interplay of the consequent phases of mixing and reaction, which in the case of fast chemical reactions is restricted by the rate of the so-called micromixing. CFD simulation of the resulting complex transport phenomenon is of great interest for researchers. Since direct numerical simulations are unrealizable for industrial-scale problems, and the space averaged approach based on large eddy simulations also has extremely high computational requirements/costs, the time averaged approaches offer themselves as a good compromise of numerical simulation tools. According to this approach, the mathematical model to be solved consists of three interdependent subsystems, namely the solution of:

1. the momentum and continuity equations (1, 2)
2. the turbulence model equation(s)
3. the transport equations of species (and heat) (3).

Mass transfer with chemical reaction in liquid-liquid systems represents an important class of chemical reactions. It has several applications such as liquid-liquid extraction, single step synthesis reactions (e.g. nitration, polymerization, trans-esterification) and biological applications (e.g. cell separation, DNA analysis, kinetic measurements, and protein crystallization). In this case the interface between two immiscible fluids plays an important role in evaluating the performance of the reactor and therefore free surface modeling is necessary. If two immiscible liquids are present in small scale channels the capillary and wall adhesion (interaction of the liquid with the solid wall) effects are more dominant and govern the flow. Different methods are available to model immiscible fluids such as the level set, volume of fluid (VOF), marker particle, lattice Boltzmann, front tracking methods and so on. A short review of these methods can be found in [1]. VOF and level set approaches belong to the most common implicit free surface reconstruction methods.

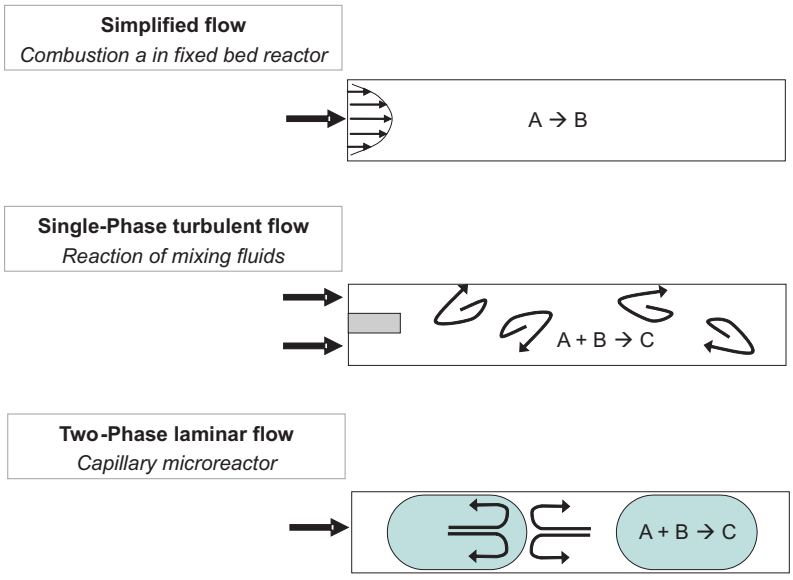

Figure 1: Common features and differences for the three case studies.

In some cases the well defined flow patterns arising due to laminar flow in liquid-liquid flows show translational symmetry in the channels which can be used to simplify the models for mass transfer and

chemical reactions in order to reduce the computational effort. Such a numerical model for mass transfer with chemical reactions for liquid-liquid flow in a microreactor was developed in [11]. The model was validated with various sets of experimental results and showed good prediction of the flow field and the mass transfer.

The present paper shortly reviews mathematical modeling and numerical simulation of single-phase, turbulent, and two-phase flows. We present three different cases (see Figure 1) with justified simplifications and necessary augmentations.

Section 2 concentrates on aspects of mathematical modeling of each test case while Section 3 presents the results of numerical simulations and compares these with experiments.

2 Mathematical modeling

2.1 Simplified flows in channels

Fixed-bed reactors are appropriate for many chemical processes especially for those involving reacting gases. Inside the cylindrical body of a fixed bed reactor the feed gas typically flows through a packed bed or channels located in a monolithic body. The surface of the solid is often coated with a catalyst enabling a heterogeneous reaction of the gas. In contrast to a standard fixed bed reactor a reverse-flow reactor (RFR) is operated under a condition of periodic flow reversal. The main advantage of the periodic flow reversal concept is that it leads to a high energy efficiency since the reactor also serves as a (regenerative) heat-exchanger. The flow reversal concept was first proposed in the nineteen thirties by [7] but first became well-known by the extensive work of Matros [2, 27].

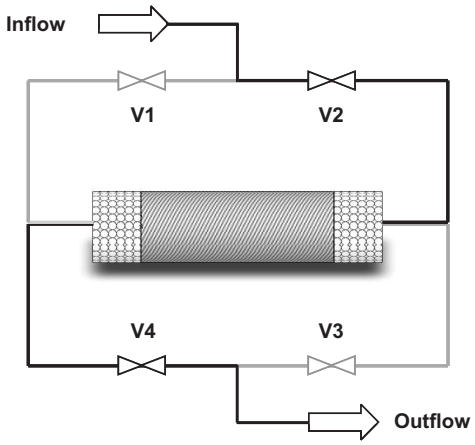

Figure 2: Schematic diagram of a reverse flow reactor. The valve pairs V1/V3 and V2/V4 are alternately opened and closed.

Since flows at low Reynolds numbers (Re) in channels tend to assume a simple flow pattern, namely the Poiseuille flow, the main focus is dedicated to model the mass and heat balance. As a result the Navier-Stokes equations were not solved explicitly. As illustrated in Fig. 3, if we consider a cut through one channel, a parabolic velocity profile $u(r)$ can be found having a maximum velocity in the center of the channel. Before the gas reacts on the catalytic surface, modeled by a reaction term r^1, it has to pass a stable boundary layer. The mass transfer resistance can by modeled by the aid of a linear coefficient β.

At higher temperatures an additional contribution from a thermal reaction (r^2) can not be excluded and thus has to be included in the model. Both reactions, $r^i (i = 1, 2)$, can locally be described by simple first order reaction kinetics according to

$$r^i(T, C) = k^i(T) \cdot C = k_0^i \cdot \exp\left[-\frac{E_A^i}{RT}\right] \cdot C \tag{4}$$

which includes a standard exponential Arrhenius temperature dependence.

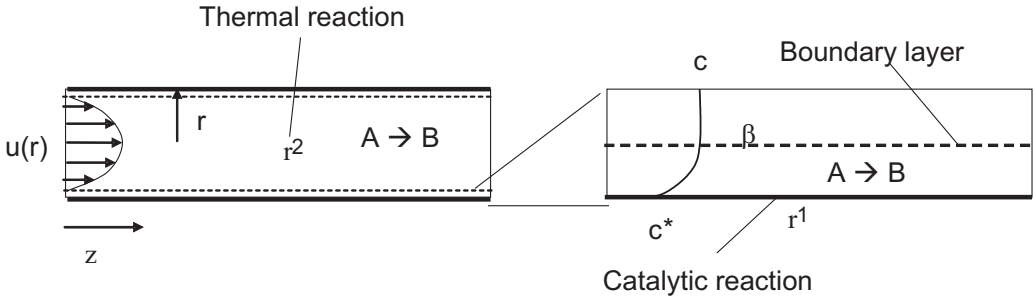

Figure 3: Poiseuille flow in a channel (left) and mass transfer through the boundary layer (right).

If a radial distribution of temperature and concentration can be neglected the general balance equation can be reduced to 1D balance equations for each phase. In those describing the gas phase we then use a mean velocity u instead of $u(r)$.

Balance equations for heat and mass over the gas phase are

$$\varepsilon(\varrho\, c_P)_g \frac{\partial T_g}{\partial t} = \varepsilon\lambda_g \frac{\partial^2 T_g}{\partial z^2} - \alpha a_v (T_g - T_s) - (\varrho\, c_P)_g u \frac{\partial T_g}{\partial z} + \Delta H_r r^2(T_g, C), \tag{5}$$

$$0 = \varepsilon D \frac{\partial^2 C_g}{\partial z^2} - \beta a_v (C - C^*) - u \frac{\partial C_g}{\partial z} - r^2(T_g, C). \tag{6}$$

In a similar way balance equations over the solid phase can be derived as

$$(1-\varepsilon)(\varrho\, c_P)_s \frac{\partial T_s}{\partial t} = (1-\varepsilon)\lambda_s \frac{\partial^2 T_s}{\partial z^2} + \alpha a_v (T_g - T_s) + \Delta H_r r^1(T_s, C^*), \tag{7}$$

$$\beta a_v (C - C^*) = r^1(T_s, C^*). \tag{8}$$

With the aid of a further simplification according to the assumptions of Vortmayer [36], one pseudo-homogeneous energy balance (9) can be obtained with $T \approx T_g \approx T_s$. We augmented (9) to also account for heat loss in order to extend the range of validity. If the catalytic reaction obeys first-order kinetics (refer (4)) the solid-phase concentration C^* is an explicit function of C and can thus be removed with the aid of (8). The resulting pseudo-homogeneous reactor model can then be represented by the following two equations

$$\varepsilon(\varrho\, c_P)_g + (1-\varepsilon)(\varrho\, c_P)_s \frac{\partial T}{\partial t} = \lambda_{\text{eff}} \frac{\partial^2 T}{\partial z^2} - (\varrho\, c_P)_g u \frac{\partial T}{\partial z} + k_{wv}(T - T^{\text{amb}}) + (-\Delta H_r) r^{1,2}(T, C), \tag{9}$$

$$0 = D_{\text{eff}} \frac{\partial^2 C}{\partial z^2} - u \frac{\partial C}{\partial z} - r^{1,2}(T, C). \tag{10}$$

Equation (9) additionally takes heat loss into account and the effective thermal conductivity λ_{eff} is computed according to Vortmayer [36]. Furthermore it can be seen that removing C^* results in a combined reaction term accounting for both types of reactions which incorporates the mass transfer resistance

$$r^{1,2}(T, C) = \left[\frac{\beta a_v \cdot k^1(T)}{\beta a_v + k^1(T)} + k^2(T) \right] \cdot C. \tag{11}$$

As a spatial boundary condition we used the common Danckwerts boundary condition. After the flow-reversal the convective terms in (9) and (10) change their signs and the spatial boundary conditions are switched. Equation (11) reveals that only the second part has got influence at elevated temperatures while at very low temperature levels the second part is negligible. The reason for this behavior is on the

one hand due to the mass transfer limitation and on the other hand due to an activation energy E_A^1 which is up to an order of magnitude smaller than E_A^2.

After numerous switchings the system reaches a so-called cyclic steady state. Within one cycle the temperature and concentration profiles move fourth and back along the z-axis. Because standard dynamical simulation approaches suffer from very slow convergence we used a direct calculation technique to speed up the computation which is described in detail in [30]. The direct calculation used here is based on a global discretization of (9) and (10). The periodicity needed for computation of cyclic steady-states was enforced by placing the following mirror symmetry boundary condition in time

$$T(z,t) = T(L-z, t+\Delta t_{cyc}). \tag{12}$$

Completing the global discretization leads to a nonlinear system of equations

$$R = \tilde{M}U + F(U) + D = 0, \tag{13}$$

where $\tilde{M}$ includes the discrete transport operator while $F(U)$ and D account for reaction and spatial boundary conditions. The solution vector U contains the nodal unknown values for the temperature T and concentration C. The nonlinear systems were solved by the Newton-Raphson method.

2.2 Single-phase turbulent reactive flows

Assuming that the physical properties of the medium subjected to the flow are more or less constant, and that the flow is incompressible, enables a solution by means of a modified version of FEATFLOW [34]. The implementation of the transport equations of species including chemical reactions (one-way coupling with flow field) and of the turbulence model (two-way coupling) is realized on top of the standard incompressible laminar flow solver. In the following sections the implementation of the developed solution algorithms for the two additional subsystems and their integration into the common framework based on FEATFLOW will be described. In this work, the modeling of turbulence was realized by the standard $k-\varepsilon$ model [24], and for chemical reactions the closure of multi-environmental micromixing model was adopted [8, 33].

2.2.1 Implementation of the $k-\varepsilon$ turbulence model

In the framework of eddy viscosity models, the hydrodynamic behavior of a turbulent incompressible fluid is governed by the Reynolds Averaged Navier-Stokes (RANS) equations for the velocity $\mathbf{u}$ and pressure p

$$\begin{aligned} &\frac{\partial \mathbf{u}}{\partial t} + \mathbf{u}\cdot\nabla\mathbf{u} = -\nabla p + \nabla\cdot\left((\nu+\nu_T)[\nabla\mathbf{u} + \nabla\mathbf{u}^T]\right), \\ &\nabla\cdot\mathbf{u} = 0, \end{aligned} \tag{14}$$

where ν depends only on the physical properties of the fluid, while ν_T is a turbulent eddy viscosity which is supposed to emulate the effect of unresolved velocity fluctuations $\mathbf{u}'$.

If the standard $k-\varepsilon$ model is employed, then $\nu_T = C_\mu \frac{k^2}{\varepsilon}$, where k is the turbulent kinetic energy and ε is the dissipation rate. Hence, the above PDE system is to be complemented by two additional mutually coupled convection-diffusion-reaction equations [24] for computation of k and ε. However, for our purposes, it is worthwhile to introduce a parameter γ

$$\gamma = \tau_T^{-1} = \varepsilon/k, \tag{15}$$

related to the turbulent time scale τ_T, which makes it possible to decouple these transport equations as follows [25]

$$\frac{\partial k}{\partial t} + \nabla\cdot\left(k\mathbf{u} - \frac{\nu_T}{\sigma_k}\nabla k\right) + \gamma k = P_k, \tag{16}$$

$$\frac{\partial \varepsilon}{\partial t} + \nabla\cdot\left(\varepsilon\mathbf{u} - \frac{\nu_T}{\sigma_\varepsilon}\nabla\varepsilon\right) + C_2\gamma\varepsilon = \gamma C_1 P_k, \tag{17}$$

where $P_k = \frac{\nu_T}{2}|\nabla \mathbf{u} + \nabla \mathbf{u}^T|^2$ is responsible for production of turbulent kinetic energy. This representation provides a positivity-preserving linearization of the sink terms, whereby the parameters ν_T and γ are evaluated using the solution from the previous outer iteration [23, 35].

The discretization in space is performed by an unstructured grid finite element method. The incompressible Navier-Stokes equations are discretized using the nonconforming $\tilde{Q}_1/Q_0$ element pair, whereas standard Q_1 elements are employed for k and ε. After an implicit time discretization by the Crank-Nicolson or backward Euler method, the nodal values of $(\mathbf{v}, p)$ and (k, ε) are updated in a segregated fashion within an outer iteration loop.

The iterative solution process is based on the hierarchy of nested loops according to the approach described in [22]. At each time step (one $n-$*loop* iteration), the governing equations are solved repeatedly within the outer k-*loop* which contains the two subordinate l-*loops* responsible for the coupling of variables within the corresponding subproblem. The embedded m-*loops* correspond to iterative flux/defect correction for the involved convection-diffusion operators. In the case of an implicit time discretization, subproblems (16) and (17) leads to a sequence of algebraic systems of the form [18, 23, 35]

$$\begin{aligned} &A(\mathbf{u}^{(k)}, \gamma^{(l)}, \nu_T^{(k)})\Delta u^{(m+1)} = r^{(m)}, \\ &u^{(m+1)} = u^{(m)} + \omega \Delta u^{(m+1)}, \end{aligned} \tag{18}$$

where $r^{(m)}$ is the defect vector and the superscripts refer to the loop in which the corresponding variable is updated. Flux limiters of TVD type are activated in the vicinity of steep gradients, where nonlinear artificial diffusion is required to suppress nonphysical undershoots and overshoots. The predicted values $k^{(l+1)}$ and $\varepsilon^{(l+1)}$ are used to recompute the linearization parameter $\gamma^{(l+1)}$ for the next outer iteration (if any). The associated eddy viscosity ν_T is bounded from below by a certain fraction of the laminar viscosity $0 < \nu_{\min} \leq \nu$ and from above by $\nu_{T,\max} = l_{\max}\sqrt{k}$, where $l_{\max}$ is the maximum admissible mixing length (the size of the largest eddies, e.g., the width of the domain). Specifically, we define the limited mixing length l_* as

$$l_* = \begin{cases} C_\mu \frac{k^{3/2}}{\varepsilon} & \text{if} \quad C_\mu k^{3/2} < \varepsilon l_{\max} \\ l_{\max} & \text{otherwise} \end{cases} \tag{19}$$

and calculate the turbulent eddy viscosity ν_T from the formula

$$\nu_T = \max\{\nu_{\min}, l_*\sqrt{k}\}. \tag{20}$$

The resulting value of ν_T is used to update the linearization parameter

$$\gamma = \tau_T^{-1} = C_\mu \frac{k}{\nu_T}. \tag{21}$$

The above representation of ν_T and γ makes it possible to preclude division by zero and obtain bounded nonnegative coefficients (required by physical reasons and program stability) without manipulating the actual values of k and ε.

To complete the problem statement the equations should be extended with initial and boundary conditions. However, for the seek of brevity the reader is referred to [22], where implementation details of the standard *wall functions* are given as well.

2.2.2 Implementation of the multi-environment micromixing model

The implementation of the multi-environment micromixing model in this work is based on the presumed joint scalar probability density function (PDF) of the form [8]:

$$f_\varphi(\psi; \mathbf{x}, t) = \sum_{i<N,\, i} p_i(\mathbf{x}, t) \Big[\prod_{\alpha<S,\, \alpha} \delta(\psi_\alpha - \varphi_\alpha^{(i)}(\mathbf{x}, t)) \Big]. \tag{22}$$

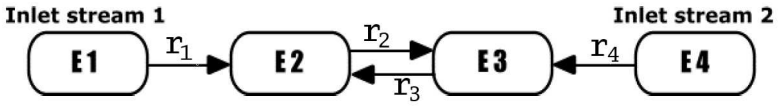

Figure 4: The scheme of inter-environmental fluxes resulting from the 4-environment decomposition of the joint PDF.

This can be interpreted as a decomposition of the full PDF into a finite set of delta functions representing a certain volume fraction containing a certain distribution of chemical species. In (22) the product is taken over all chemical species α, and the sum over all environments i. Conceptually the model enables the computation of the premixed and non-premixed environments i in sense of time averaged probabilities p_i by introducing general transport equations governing their evolution in time and space

$$\frac{\partial p_i}{\partial t} + \nabla \cdot \left(p_i \mathbf{u} - \frac{\nu_T}{\mathrm{Sc}_T} \nabla p_i \right) = P_{p_i}, \quad i = 1 \text{ to } N. \tag{23}$$

Here the sink/source term P_{p_i} on the right-hand side expresses the rate of micromixing to/from the neighboring environments $i-1$ and $i+1$ and is related to the probability flux r_j for the given environments $j \in [i-1, i, i+1]$. Due to the conservation of probabilities the following two relations hold

$$\sum_{i<N,\, i} P_{p_i}(r_{i-1,i,i+1}) = 0 \quad \text{and} \quad p_j = 1 - \sum_{i<N,\, i,\, i\neq j} p_i = 0, \tag{24}$$

where the first equation constrains the net production of environments and the second makes it possible to express one of the environments as a linear combination of the others.

The adopted closure model possesses two important properties [8, 13] from the point of view of the probability fluxes. First of all, these fluxes are responsible for the mutual coupling between the transport equations (23), and secondly they are scaled by the turbulent time scale τ_T defined by the turbulence model (15,21)

$$r_i = C_\varphi \tau_T \quad \text{with} \quad C_\varphi \in [1, 2]. \tag{25}$$

The last set of transport equations needed to be introduced involves the evolution of chemical species in terms of their volume fractions s_α in a referenced environment (i) and has the following form

$$\frac{\partial s_\alpha^{(i)}}{\partial t} + \nabla \cdot \left(s_\alpha^{(i)} \mathbf{u} - \frac{\nu_T}{\mathrm{Sc}_T} \nabla s_\alpha^{(i)} \right) = P_{s_\alpha^{(i)}} + R_{s_\alpha^{(i)}}. \tag{26}$$

The first sink/source term on the right hand side has the same physical meaning as in (23), while the second one represents the fluxes in the discrete space of chemical species due to chemical reactions. The conservation law constrains these fluxes as well as the volume fraction of species in the following form

$$\sum_{\alpha<S,\, \alpha} P_{s_\alpha^{(i)}} = P_{p_i}, \quad \sum_{\alpha<S,\, \alpha} R_{s_\alpha^{(i)}} = 0, \quad \text{and} \quad s_\beta^{(i)} = 1 - \sum_{\alpha<S,\, \alpha,\, \alpha\neq\beta} s_\alpha^{(i)} = 0. \tag{27}$$

The discretization of the above presented PDEs is performed by the standard Q_1 element in space and by the second order Crank-Nicolson method in time. A 4-environment decomposition is applied for the joint PDF (see Fig. 4), which for a system with two separated inlet streams gives rise to the following system of micromixing fluxes

$$\begin{pmatrix} P_{p_1} \\ P_{p_2} \\ P_{p_3} \\ P_{p_4} \end{pmatrix} = \begin{pmatrix} -r_1 & & & \\ +r_1 & -r_2 & +r_3 & \\ & +r_2 & -r_3 & +r_4 \\ & & & -r_4 \end{pmatrix}. \tag{28}$$

In general, each of the inlet streams, represented by the side environments in Fig. 4, contain just one of the chemical species needed for the chemical reaction, therefore the side-environments 1 and 4

are free of chemical reactions. The role of these environments is to supply the middle environments by means of micromixing thus enabling the chemical reaction(s) to take place. Since the computation of (23) and (26 depends on the flow field and on the turbulent time scale, their solutions are realized last for each given time step [28]. The system of equations (23) and (26) subjected to FEM-TVD results in a non-linear algebraic system of the form:

$$A(g^{(l+1)})g^{(l+1)} = B(g^{(l)})g^{(l)} + q^{(k)}, \quad l = 0, 1, 2, ... \tag{29}$$

where $g = (p_i, s_\alpha^{(i)})$ and $q^{(k)}$ is the combination of sources and sinks evaluated by means of the values from the previous time step k. The discrete operators A and B are as follows

$$A(g) = M_L - \theta\Delta t(K(g) + D) \quad \text{and} \quad B(g) = M_L + (1-\theta)\Delta t(K(g) + D), \tag{30}$$

where M_L is the lumped mass matrix, K is the discrete convection matrix subjected to discrete upwinding [18], and D is the discrete diffusion operator. Note that without additional treatment $q^{(k)}$ (due to the contribution of the sink terms) poses a hazard to preserving the positivity of the numerical scheme. Prevention of such a behavior is performed by limiting the individual sink terms arising by micromixing effects or due to chemical reactions respectively. The limiting is then based on the linearly approximated maximal consumption rate evaluated by the maximum amount of consumable material available for the given time step. Then, in case of micromixing, the following applies

$$r_i = \min((M_L p_i/\Delta t), r_i). \tag{31}$$

A similar constraint is related to the minimal volume fraction of reactant(s) required for a given chemical reaction

$$\xi_\alpha^{(i)} = \min(\min(M_L s_\alpha^{(i)}/\Delta t), \xi_\alpha^{(i)}) \quad \alpha \in \text{reactants}. \tag{32}$$

For sufficiently small time steps (31) and (32) ensures the desired performance of the numerical scheme.

2.3 Two-phase laminar flows

2.3.1 Free surface modeling

The starting point for fluid flow modeling is the governing equations for momentum and mass transport. For fluid flows that can be assumed to be incompressible the Navier-Stokes equations are applicable

$$\rho_i(\frac{\partial \mathbf{u}}{\partial t} + (\mathbf{u}\cdot\nabla)\mathbf{u}) + \nabla p - \nabla\cdot(\mu_i(\nabla\mathbf{u} + \nabla\mathbf{u}^T)) = \rho_i\mathbf{f}, \qquad \nabla\cdot\mathbf{u} = 0 \tag{33}$$

for each of the fluid phases i. Alternatively one might, since the same equation is used for all phases, pose the following problem

$$\rho(\mathbf{x})(\frac{\partial \mathbf{u}}{\partial t} + (\mathbf{u}\cdot\nabla)\mathbf{u}) + \nabla p - \nabla\cdot(\mu(\mathbf{x})(\nabla\mathbf{u} + \nabla\mathbf{u}^T)) = \rho(\mathbf{x})\mathbf{f}, \qquad \nabla\cdot\mathbf{u} = 0 \tag{34}$$

where now the density $\rho(\mathbf{x})$ and viscosity $\mu(\mathbf{x})$ depend on the position and the location of the phases. Boundary conditions for velocity and stresses as well as initial conditions further specify the problem. Additionally we might also have special conditions on the interfaces separating the different fluids, so called interfacial boundary conditions, of which the most common reads

$$[\mathbf{u}]|_\Gamma = 0, \quad -[-p\mathbf{I} + \mu(\nabla\mathbf{u} + \nabla\mathbf{u}^T)]\big|_\Gamma \cdot \hat{\mathbf{n}} = \sigma\kappa\hat{\mathbf{n}} \tag{35}$$

where $\hat{\mathbf{n}}$ denote the interface normal and $[\mathsf{A}]|_\Gamma$ is the jump of property A across the interface Γ. These conditions imply continuity of the velocity across the interface and also a jump in the normal stress proportional to the coefficient of surface tension σ and the curvature of the interface κ. The interface conditions may be rewritten as volumetric forces and then take the form

$$\mathbf{f}_{st} = \sigma\kappa\hat{\mathbf{n}}\delta(\Gamma, \mathbf{x}). \tag{36}$$

The modeling approach described above naturally requires that an additional method is used to track and separate the respective phases, a so called interface tracking method. There are in general two schools of thought available here, on the one hand one can employ very accurate Lagrangian methods, where the grids are always aligned with the interfaces separating the different phases, or Eulerian methods, where the different phases may move arbitrarily over the grids thus allowing one even to use fixed grids.

The Lagrangian approach is generally very accurate since the phases are captured perfectly by the grid (no interfaces ever intersect the grid cells). When an interface moves, the connecting grid points move with the interface while grid points in the interior of the domain will have to be distributed efficiently according to some given rules. Such an algorithm is denoted an arbitrary Lagrangian Eulerian (ALE) approach where the governing equations are altered to account for the grid motion. In the simplest form the ALE formulation of the Navier-Stokes equations simply subtracts the grid velocity $\mathbf{w}$ from the velocities in the convective term $((\mathbf{u}-\mathbf{w})\cdot\nabla)\mathbf{u}$. The major difficulty with these approaches is that the grids become very computationally inefficient for large changes in topology requiring remeshing which can lead to mass loss. In addition, effects such as break up and merging of interfaces need to be treated manually according to some predefined rules.

The Eulerian approach is in general easier to implement when using fixed grids and thus frequently leads to less CPU time. Complex topology change of the interfaces/phases is usually also handled automatically by these interface tracking algorithms. Most of these approaches typically smear out the interface effects over a region of a few cell sizes and this naturally compromises the accuracy that can be obtained. One remedy to counter this negative effect is to either locally and dynamically refine the grids in the regions of interest or possibly redistribute the grid nodes to more favorable locations. The latter option will naturally again call for the ALE formulation of the governing equations.

To highlight the differences of these two approaches we present two calculations of rising bubbles computed for a benchmark study. The first bubble undergoes very minor topology change, and as can be seen from Figure 5(a) both the calculation with a Lagrangian code and an Eulerian code agree perfectly well. The big difference is that about 5000000 unknowns (820000 cells) were required to obtain this accuracy for the Eulerian code while only about 100000 unknowns were required for the Langragian approach. This was naturally also reflected in the CPU times where the Lagrangian code was 5 times faster than the Eulerian code. The second bubble, shown in Figure 5(b), obviously undergoes severe topology change. Here the Eulerian code predicts bubble separation/break up which the Lagrangian code will never do irrespective of how much deformation takes place.

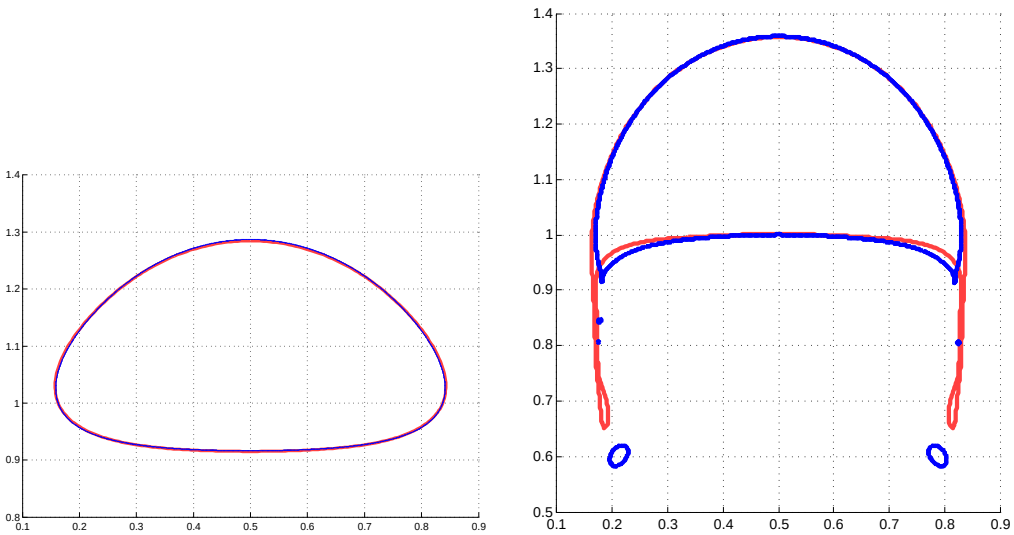

(a) Re=35, Eo=10, ρ_1/ρ_2=10, μ_1/μ_2=10 (b) Re=35, Eo=125, $\rho_1/\rho_2 = 10^3$, $\mu_1/\mu_2 = 10^2$

Figure 5: Predicted bubble shapes for a low density/viscosity ratio bubble (a) compared to a high density ratio one (b). The results from a Lagrangian body fitted mesh code is seen in red and from an Eulerian level set code in blue.

The two most commonly used Eulerian volume tracking methods is the volume of fluid (VOF) method by Hirt and Nichols [12] and the more recently devised level set method by Osher and Sethian [31]. They both share the common characteristic that an additional scalar field is used to identify the different fluid phases. The VOF method uses a discontinuous so called volume fraction which is unity in cells with one phase and zero in the other. Thus cells with an intermediate volume fraction have an interface segment intersecting them. Since the VOF function does not explicitly indicate the location of the interface it must be reconstructed in each time step for which various algorithms have been devised. The level set method on the other hand uses a continuous function to identify the phases, a level set is defined (usually taken as the zero contour/surface) and the different fluids exist on the different sides of this level set. The advantage here compared to VOF is that the chosen level set uniquely identifies the position of any interface. Geometric quantities such as normals and curvature can also be reconstructed both easily and globally. The governing equation transporting the scalar VOF or level set functions is a standard convection equation of the form

$$\frac{\partial f}{\partial t} + \nabla \cdot (\mathbf{u} f) = 0 \tag{37}$$

where the convective velocities are given by the flow equations (34). The flow velocities are coupled to the interface tracking equation and the VOF/level set function f is implicitly coupled to the flow equations via the density, viscosity, and also possibly the interfacial boundary conditions. The solution of the scalar transport equation can be done completely mass preserving for the VOF method (in some sense anyway, since the interface is not uniquely defined one might argue whether this is true or not) unlike for the level set method where this is not possible. Another drawback of the level set method is that the level set function generally will distort in some complex flow regions necessitating periodic reinitialization adding to algorithmic complexity and possible solution distortions.

The solution of the above methods and equations is up to the implementer. In fact all of the usual space discretization methods are applicable; finite differences, volumes, and elements all apply, except that perhaps finite differences are not the first hand choice when dealing with non tensor product grids. In particular we would like to emphasize the option of using the level set method as an interface tracking algorithm together with finite elements for the discretization in space. This allows for a rather elegant reformulation of the surface tension forces which is fully implicit with respect to the interfaces (they need not be found explicitly), allows for larger time step sizes, and does not necessitate the computation of curvature [14]. The finite element method also allows for unstructured grids to be used and thus also the grid deformation approach which has the potential to increase accuracy while still keeping low computational costs and the ease of implementation.

2.3.2 Immiscible fluids in microchannels

Immiscible liquids in the laminar flow regime are of particular interest due to the well-defined interfacial area for mass transfer which helps for *a priori* predictions of the mass transfer rates. Currently, more and more efforts are being made to use laminar flow in microreactors in order to increase the transfer rates, to reduce the energy consumption, and to enhance safety. Two major flow regimes arise depending on the wall adhesion and interfacial tension: parallel flow and drop (slug) flow. The slug flow shows enhanced mass transfer due to very high interfacial area and intense internal circulations within the slugs due to shearing action between slug axis and capillary wall/continuous phase.

The transition between both flow regimes depends on the angle of contact of the two liquids, interfacial tension, and wall adhesion. If the surface tension between the discrete phase and the wall material is higher than the interfacial tension between two liquids, they flow alternatively in the small scale geometries, otherwise one of the liquids flows in the form of enclosed slugs. This only happens in the case of liquid-liquid two phase flows. In alternate flow, rather than imposing the boundary conditions at the wall itself, the contact angle that the fluid assumed to make with the wall is used to adjust the surface normal in the cells near the wall. The contact angle values are taken from experimental measurements and no-slip boundary conditions (zero velocity on walls) are used. The liquid-liquid-solid contact line moves along the wall, presenting a kind of singularity [9]. In this case, the velocity of the faces adjacent

to the wall are kept to zero and other parts (cell center and other faces) have non-zero velocity. Such non-zero velocities influence the volume fraction field and therefore also the position of the interfaces. Thus, such an implementation realizes the movement of the liquid-liquid-solid contact line despite specifying no-slip boundary conditions at the solid surface.

2.3.3 Simplified model

In the case of interfacial mass transfer and chemical reactions, the above methodology can be extended by adding appropriate equations for the species transport. The time required for reactions or mass transfer is however often large and requires a long reactor length. The aspect ratio of the geometry is very large and requires huge numbers of cells (to maintain the aspect ratio of cells equal to 1) and thus also a lot of computational resources to completely solve the problem. In the case of liquid-liquid flows, the patterns are relatively well-defined because both liquids exert considerable shear on each other and thus we can assume a stationary interface to simplify the model. In the case of slug or drop flow in the small channels or capillaries, we can also assume translational symmetry which can reduce the computational resources significantly. Such a numerical model was developed to describe the internal flow patterns within the fluid segments by Harries *et al*. [11] and the transfer of the dissolved chemical species within and across the segments for liquid-liquid slug flow. The flow was represented by two stagnant, adjacent rectangular units which are linked at both ends to form a continuous loop. The model was validated with various sets of experimental results and showed good prediction of the flow field and mass transfer.

3 Applications and results

3.1 N_2O-decomposition in a reverse-flow-reactor

The validation of the model described in section 2.1 is based on the hybrid N_2O-decomposition which has been experimentally studied in our group in a technical scale RFR [29]

$$2N_2O \rightarrow 2N_2 + O_2 \qquad \Delta H_r = -163 \quad kJ/mol. \tag{38}$$

In this context the expression ”hybrid” means that in addition to a catalytic decomposition of N_2O a thermal decomposition also takes place at higher temperatures. The applied catalyst is a Platinum/Rhodium complex wash-coated in a ceramic monolith block containing hundreds of channels. Irrespective of the reaction pathway the N_2O-decomposition is an irreversible and exothermic reaction. Since the thermal reaction dominates in the free gas phase and the catalytic reaction occurs on the surfaces of the wash-coat the hybrid N_2O-decomposition is covered by the mathematical model presented in section 2.1.

The duration of each experiment was rather long due to the dominating thermal inertia of the solid material. From start up of the RFR it took 24-48 hours until the cyclic steady-state was reached. Even after slight changes in operation parameters, e.g. increase of the feed gas concentration, it took hours until the system relaxed to a new cyclic steady-state from one cyclic steady-state. Unfortunately, there is no experimental speed up technique corresponding to direct numerical simulation. Measurement data could be collected with the aid of 20 temperature sensors along the main axis and an O_2-analyzer located at the outflow.

The numerical simulation was based on a direct calculation of cyclic steady-states. The spatial terms in (10) and (9) were discretized with central differences (CDS) for the diffusive parts and a second order upwinding scheme (linear upwind differencing scheme; LUDS) for a robust treatment of the convective parts. The time derivative in (9) was treated with Crank-Nicolson. We used 100 grid points in space and 50 in time. In combination with the mentioned spatial boundary condition according to Danckwerts and the temporal boundary condition in equation (12) a stationary reformulation (13) can be achieved. We included a path continuation algorithm in order to efficiently compute numerous solutions. More details can be found in references [30] and [32]. A typical switching time is about a few hundred seconds. The axial length of the studied RFR was $L = 1.5$ meters.

Table 1: Physical and chemical parameters (for average mass fraction $w_{N_2O} = 0.1$, reference temperature $T = 500\,^{\circ}C$).

symbol	value	unit	symbol	value	unit
βa_v	198.0	$[\frac{m^2}{m^3}]$	k^1_{0,N_2O}	$4.1 \cdot 10^8$	$[\frac{1}{s}]$
L	1.5	$[m]$	E^1_A	151.0	$[\frac{kJ}{mol}]$
D_{eff}	$6.91 \cdot 10^{-3}$	$[\frac{m^2}{s}]$	k^2_{0,N_2O}	$1.1 \cdot 10^{10}$	$[\frac{1}{s}]$
λ_{eff}	0.85	$[\frac{W}{mK}]$	E^2_A	251.0	$[\frac{kJ}{mol}]$
u	0.4	$[\frac{m}{s}]$	ΔH_r	$-81.6 \cdot 10^3$	$[\frac{J}{mol}]$
k_{wv}	30.0	$[\frac{W}{m^2K}]$	R	8.3144	$[\frac{J}{molK}]$
$\varepsilon(\varrho\, c_P)_g + (1-\varepsilon)(\varrho\, c_P)_s$	$428.7 \cdot 10^3$	$[\frac{J}{m^3K}]$	$(\varrho\, c_P)_g$	531.0	$[\frac{J}{m^3K}]$

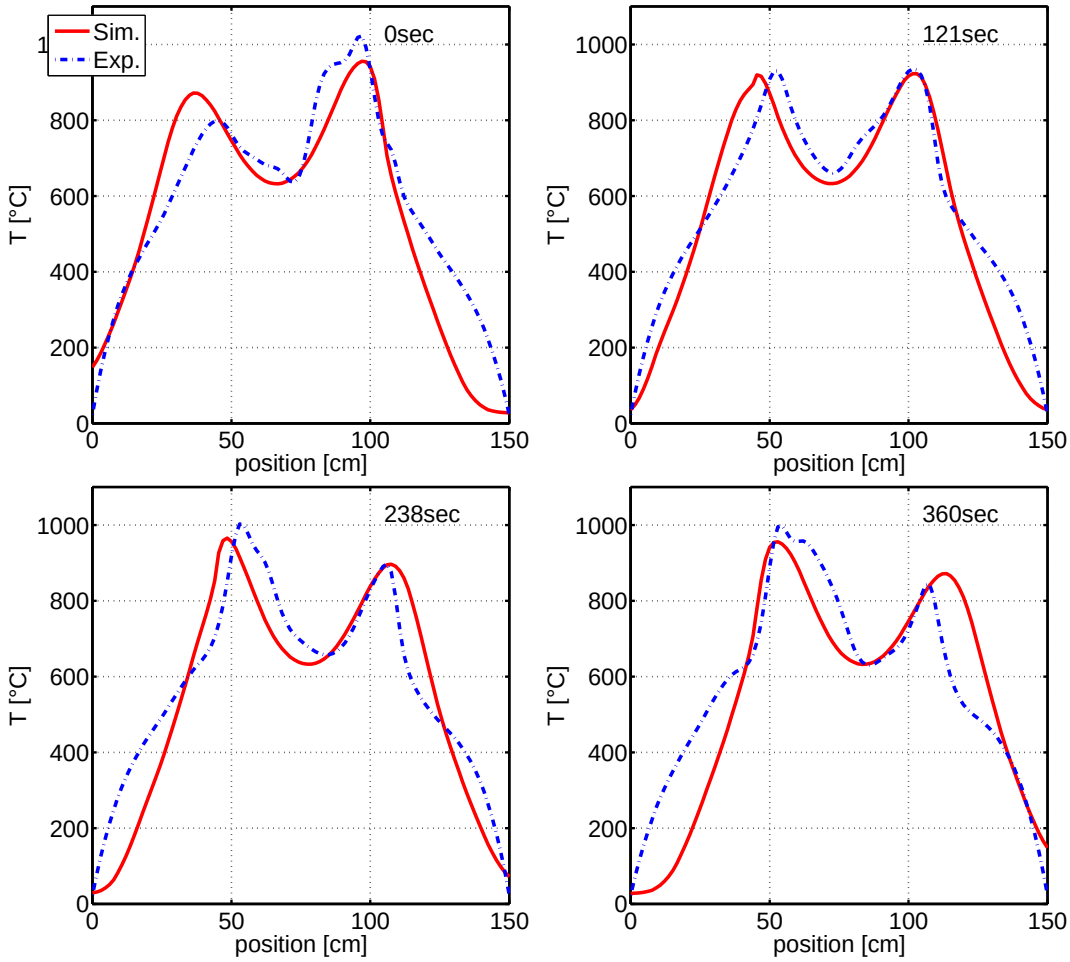

Figure 6: Comparison of simulation and experiment for $t_{rel} = 0s, 121, 238, 360\ s$.

Fig. 6 shows a comparison between an experiment and a simulation for an inlet concentration of $C = 2.4\ mol/m^3$ and a switching time of $\Delta t_{cyc} = 360s$. A good match between the temperature values calculated and the experimental data can be found. The four inserts show different snapshots for various

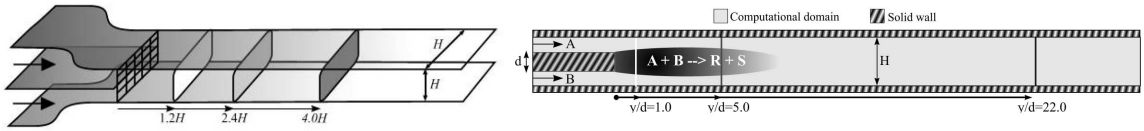

Figure 7: Sketch of the geometry for the experiments of Komori [17] (left) and Hjertager [13] (right).

times during a half cycle and enable us to conclude that the temperature profiles qualitatively exhibit the same shape in space and time. The M-shape of the temperature profiles and the maximum and (local) minimum temperatures are predicted very well. Two obvious differences emerge though. On the one hand the calculated temperature fronts move faster and over a wider range than what was observed in the experiments. On the other hand it is apparent that the curvature of the profiles deviates considerably in the outer heating zones. The reason for this inconsistency can be found in the assumption of constant gas velocity and porosity in the model equations.

3.2 Turbulent reacting flows

Validation of the model presented in Section 2.2 was achieved in two steps starting with the turbulence model and followed by the reaction (micromixing) model [28]. For the validation of the $k-\varepsilon$ turbulence model the reader is referred to [20], where reattaching flow over a backward facing step was simulated which resulted in good agreement with other referenced computational studies. The performance of the implemented multi-environment micromixing model was analyzed on two different test cases supported by experimental data [13, 17]. The investigated acid-base neutralization reaction in both cases was the following

$$\overset{\mathrm{A}}{\mathrm{CH_3COOH}} + \overset{\mathrm{B}}{\mathrm{NH_4OH}} \longrightarrow \overset{\mathrm{R}}{\mathrm{CH_3COONH_4}} + \overset{\mathrm{S}}{\mathrm{H_2O}},$$

which corresponds to the reaction rate constant $k_v^{\infty} \approx 10^{15}\mathrm{m^3mol^{-1}s^{-1}}$. Our first geometrically simpler example deals with the simulation of Komori's experiment [17], where both of the reactants were introduced in an equi-molar ratio into the water tunnel by separate inlet streams (see Fig. 7) in a form of aqueous solutions. The experimental data were measured for two cases of operational conditions; for non-reacting flow (inert mixing of one of the reactants) and for reacting flow (mixing and chemical reaction). Hereby, the data obtained by non-reacting conditions makes it possible to validate the performance of the implemented turbulence model. The three vertical cross-planes at Fig. 7-left represents the locations where the concentration profiles of the reactant A were measured. A mesh was used at the entrance of the water tunnel to maintain isotropic turbulence of the flow characterized by $Re = 25000$ with respect to H. The measured and computationally predicted concentration profiles for non-reacting and reacting operating conditions are presented in Fig. 8, where comparisons are made for three distances from the mesh. As can be seen from the figure a small discrepancy can be observed in the vicinity of the wall for the reacting flow case. This can be attributed to the usage of wall functions instead of integration of the model equations down to the wall with an appropriate Low-Reynolds model. Anyway, the predictions agree well with the measured data [17] as well as with computational results of other studies [33].

Our next numerical example corresponds to a geometrically more complex problem, which was experimentally and computationally processed by Hjertager [13]. The scheme including the geometry, situation of feed streams and sampling planes are demonstrated in Fig. 7 (right). Experimental data were measured [13] for three cases of inlet flowrate ratios ($\dot{V}_A/\dot{V}_B \in [1.0, 0.5, 0.25]$) corresponding to $Re = 6600, 4950$ and 4125 based on the main channel hydraulic diameter) for non-reacting and reacting conditions (except for $\dot{V}_A/\dot{V}_B = 0.25$). Since the experimental set-up involved a long entrance channel for both of the reactants, the given flowrates for the simulations were imposed as fully developed turbulent inflow boundary conditions. The comparison of our simulated mesh independent results with the experimental data for the middle velocity ratio is given in Fig. 9. The verification of the computed velocity profiles for the non-reacting case according to the experimentally obtained data confirms a good agreement (Fig. 9-left). This is also confirmed by the comparison of concentration profiles for the inertly

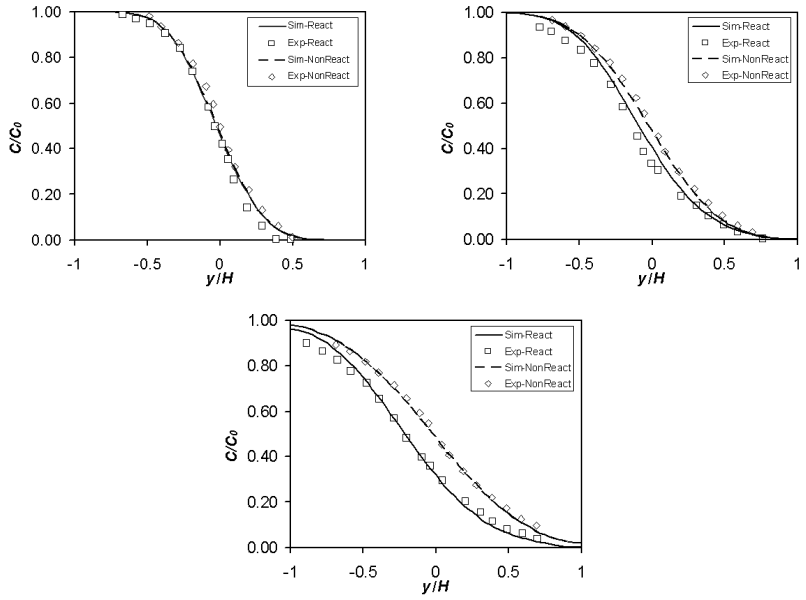

Figure 8: Normalized concentration profiles of reactant A at different distances from the mesh (from left to right, $1.2H, 2.4H$ and $4.0H$) for the experiment of Komori [17].

mixed material A (Fig. 9-middle). Moreover, the predictions of the implemented micromixing model correlates reasonably well with the measured and computationally predicted data of Hjertager (see Fig. 9-right).

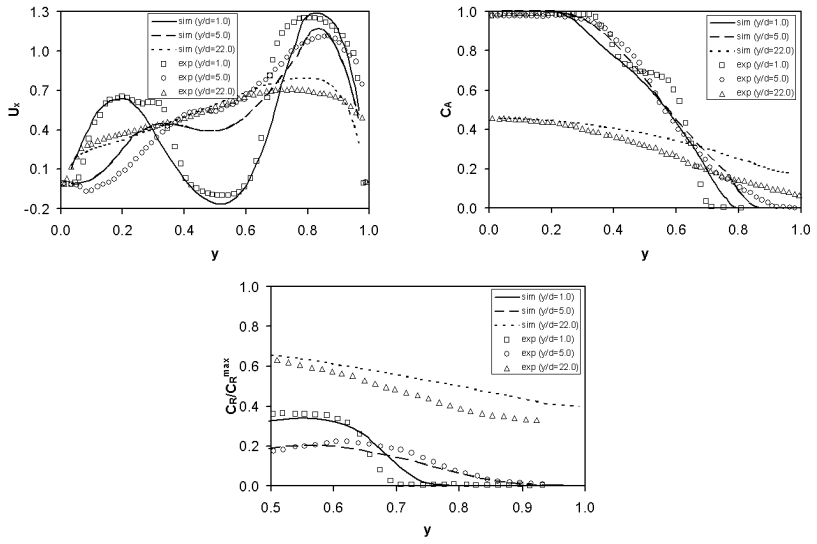

Figure 9: Comparison of computationally and experimentally [13] obtained data for Hjertager's experiment at different distances behind the feed stream separating obstacle.

3.3 Capillary microreactor

To study two phase laminar flow we consider the example of liquid-liquid slug flow in a capillary. It is defined as an alternating flow of one phase separated by the other.

The slug flow is generated by introducing two immiscible liquids into a Y-junction. One liquid initially flows downstream through the junction, while the other penetrates over to the opposite side of the junction, this mutual displacement process generates the characteristic alternating slug flow structure.

In order to generate the slug flow by CFD methodology, the simulations were carried out for the same experimental operating conditions using different immiscible fluid systems. As a first attempt, two sinusoidal inputs were given for two phases in order to understand if the hydrodynamic instabilities are one of the reasons to generate the slug flow. Initially, the simulations were carried out without surface tension and wall adhesion. In this case, at low flow velocities, both phases flow parallel to each other with wavy interface. With further increase in the flow velocities of both phases, the waves grow and finally each wave was as big as a slug. The connecting layer between two slugs was found to be reduced along the length of the capillary. Then the surface tension was implemented and identical flow rates were given. It was observed that the secondary phase flows in the form of deformed drops which had no interaction with the wall. Finally, wall adhesion was implemented by explicitly defining the wall contact angle from experimental measurements (80^o - 90^o) and well-defined slug flow was observed. The effects of various operating conditions on the slug flow generation are given in [15]. One of the results using level set method is shown in Fig. 10.

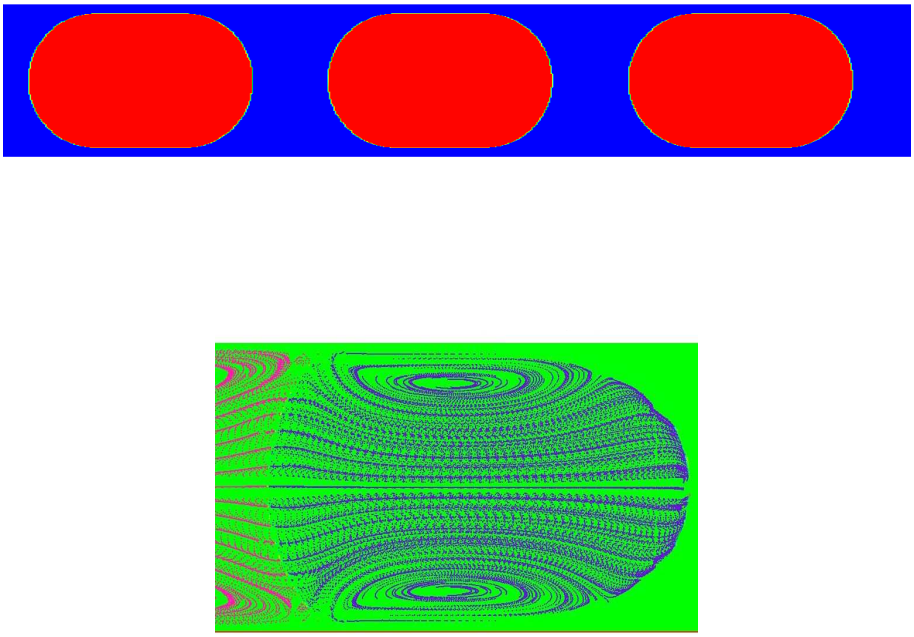

Figure 10: Two phase slug flow in a capillary simulated using level set method and internal circulation within the slugs.

A CFD model was furthermore developed based on translational symmetry to study the mass transfer with and without chemical reactions. The two extreme ends of the domain were connected using periodic boundary conditions and the interface between the two slugs was made using the moving boundary concept. Several simulations with different geometries and operating conditions with various viscosity combinations were carried out to study the flow behavior within the slugs. Although the viscosities of two slugs were different, both slugs showed similar velocity profiles for a given set of operating conditions. However, with a change in the flow velocity, an increased intensity of internal circulations was observed. The independence of viscosity on flow patterns in this case is due to the very low Reynolds number where the flow behaves as Stokes flow. It makes the mathematical modeling relatively easy as one can assume equal viscosity in both slugs.

For the mass transfer studies undertaken in such systems, additional equations of species transport are

solved for each species. The solution ends with equal concentration in both phases for a given species, which is not the general case in the physical system. This discontinuity should be treated by making the transformations given by Yang and Mao [37] which imposes an equal concentration condition at the interface. In order to reduce the computational effort, it is important to carry out simulations in a transient manner i.e. simulations are first carried out for solving steady state velocity and pressure and then they are switched for the species transport calculations. This is because of lower time requirements for the first part of the simulations and more time requirements for latter part. Before calculating the actual variables/parameters, it is important to make the solution grid independent. Two types of mesh configurations can be used in the case of a structured mesh: an uniform mesh in the whole domain and a more refined mesh in the vicinity of the interface. The later part shows more advantage as it reduces the total number of cells required to achieve a mesh independent solution.

In the case of chemical reaction, it is important to identify the reaction medium for defining the source and sink terms. In this region, the convection-diffusion-reaction equations are solved for each species taking part in the reaction. The convection-diffusion-reaction equations are solved using a straight-forward operator splitting strategy described in [21], i.e. first of all scalar quantities are transported without taking the source/sinks into account. The convection-diffusion equations of each species are processed in parallel and the updated concentrations were used as initial data for a system of reaction ODEs, which describes the accumulation and consumption of a particular species. It is important to note that the operator splitting strategy was applied locally in time, i.e. within each time step $\triangle t_n$. The first part of the equation is solved similar to the Navier-Stokes equations while the second part is solved depending on the nature of reaction. The concentrations which were obtained in the solution of convection-diffusion equation were used as initial data for the solution of ODEs. For slow reactions with very low value of rate constants, the ODEs can be solved using explicit treatment. However, for fast or rapid reactions, in a given time step the explicit method produces very high but non-realistic values of the updated concentration of the products. This problem could be solved using a very small time step, but this is not feasible, because the computational time will increase significantly. Therefore an implicit treatment is necessary to solve such problems. The snapshot for simulated concentration profiles for a neutralization reaction

$$\overset{\mathrm{A}}{\mathrm{CH_3COOH}} + \overset{\mathrm{B}}{\mathrm{NaOH}} \longrightarrow \overset{\mathrm{R}}{\mathrm{CH_3COONa}} + \overset{\mathrm{S}}{\mathrm{H_2O}},$$

is shown in Figure 11. The experimental validation and modeling details are presented in [16].

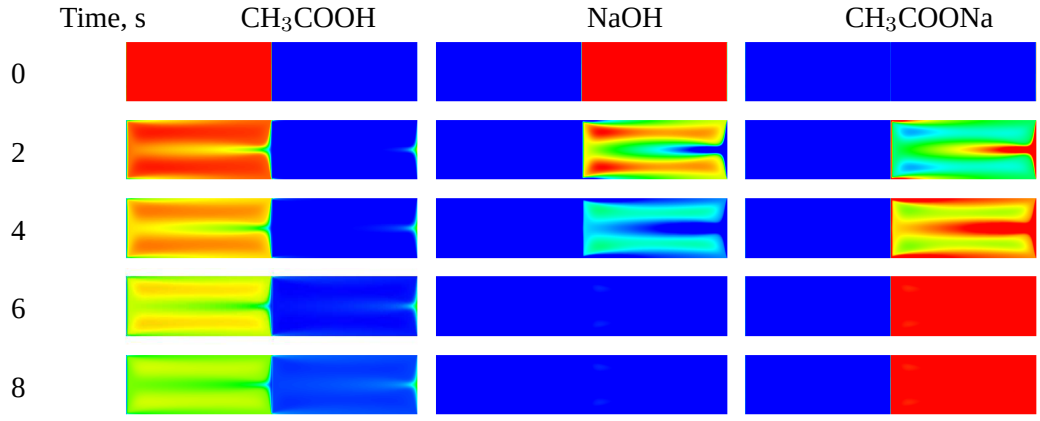

Figure 11: Snapshots of concentration profiles of CH_3COOH, NaOH, and CH_3COONa (slug length = 1.9 mm, slug flow velocity = 3.33 mm/s). CH_3COOH diffuses through the interface from one phase to the other and reacts with NaOH to form CH_3COONa and H_2O.

4 Conclusions

A detailed understanding of the underlying flow pattern is necessary when designing a chemical process. The flow is responsible for the distribution of mass, momentum and energy inside the apparatus. If the flow field can be simply described or tends to assume an analytical solution the Navier-Stokes equation need not be solved explicitly. On the other hand if the flow is turbulent or is influenced by different phases then additional model equations must be taken into account.

Chemical processes carried out in fixed beds are usually mathematically described based on simplified 2D or even 1D models without solving the flow field. We have elaborated a simplified 1D model comprising of merely one mass balance and one heat balance. The presented example of the N_2O-decomposition in a fixed bed operated under periodical flow reversals exhibits a slow transient behavior when treated with standard dynamical simulations. That is why we utilized the direct calculation method as a speed up technique for the calculation of cyclic steady-states. The comparison of the simulated temperature and concentration profiles with corresponding experiments shows a qualitative good agreement although only temperatures could be directly compared.

The problems associated with fast chemical reactions limited by mixing are different. Here, the appropriate description of the macro and micro mixing effects are essential when physically realistic and correct results are desirable. For this reason the combination of the $k - \varepsilon$ model and multienvironment micromixing model was utilized. Both of the implemented models were subjected to validation with respect to experimental results. Comparison of the obtained results in the range of validity of the model for geometrically simpler as well as for more complex problems confirmed the predictability and robustness of the designed simulation tool. However, modifications related to the turbulence model in sense of accurate boundary layer modeling is still required.

In the third case, two phase laminar flows, different modeling aspects for modeling of hydrodynamics, mass transfer and chemical reactions are presented. Liquid-liquid two phase flow in small scale geometries, due to considerable shear by one phase on the other, show well-defined flow patterns giving an opportunity to simplify the model by assuming a fixed interface condition which requires less computational resources. The detailed methodology presented in this part is useful to develop models with moving or fixed interface under laminar flow conditions.

References

[1] M. van Sint Annaland, W. Dijkhuizen, N. G. Deen and J. A. M. Kuipers, *Numical simulation of behaviour of gas bubbles using a 3D front tracking method*, AIChE Journal, **52**(1), 2006, pp.99-110.

[2] G. Boreskov, Y. S. Matros, *Unsteady-state performance of heterogeneous catalytic reactions,* Catalysis reviews, Science and Engineering, **25**(4), 1983, pp.551-590.

[3] D. Bothe, M. Koebe, K. Wielage and H. J. Warnecke, *VOF simulations of mass transfer from single bubbles and bubble chains rising in the aqueous solutions,* Proceedings of FEDSM 03: 4th ASME-JSME Joint Fluids Engineering Conference, Honolulu, Hawaii, USA, 2003.

[4] J. U. Brackbill, D. B. Kothe and C. Zemach, *A continuum method for modelling surface tension,* Journal of Computational Physics, **100**(2), 1992, pp.335-354.

[5] G. Cerne, S. Petelin and I. Tiselj, *Coupling of the interface tracking and the two-fluid models for the simulations of incompressible two phase-flow,* Journal of Computational Physics, **171**(2), 2001, pp.776-804.

[6] L. Chen and Y. Li, *A numerical method for two-phase flows with an interface,* Environmental modelling and software, **13**, 1998, pp.247-255.

[7] F. G. Cottrell, *Purifying gases such as those from incinerators,* 1938, Patent US 2121733.

[8] R. O. Fox, *On the relationship between Lagrangian micromixing models and computational fluid dynamics,* Chemical Engineering and Processing **37**(6), 1998, pp.521-535.

[9] P. R. Gunjal, V. V. Ranade and R. V. Chaudhari, *Dynamics of drop impact on solid surface: experiments and VOF simuations,* AIChE Journal, **51**(1), 2005, pp.59-78.

[10] S. Hardt and F. Schonfeld, *Simulation of hydrodynamics in multiphase microreactors,* Fifth World Congress on Computational Mechanics, Vienna, Austria, 2002.

[11] N. Harries, J. R. Burns, D. A. Barrow and C. Ramshaw, *A numerical model for segmented flow in a microreactor,* International Journal of Heat and Mass Transfer, **46**(17), 2003, pp.3313-3322.

[12] C. W. Hirt, and B. D. Nichols, *Volume of fluid (VOF) method for the dynamics of free boundaries,* Journal of Computational Physics, **39**(1), 1981, pp.201-225, (DOI: 10.1016/0021-9991(81)90145-5).

[13] L. K. Hjertager, *Experimental and Computational Study of Mixing and Fast Chemical Reactions in Turbulent Liquid Flows*, Ph.D. Thesis, Aalborg University, Esbjerg, 2004.

[14] S. Hysing, *A new implicit surface tension implementation for surface tension flows*, International Journal of Numerical Methods in Fluids, **51**(6), 2006, pp.659-672, (DOI: 10.1002/fld.1147).

[15] M. N. Kashid, F. Platte, D. W. Agar and S. Turek, *Computational modelling of slug flow in a capillary microreactor, Journal of Computational and Applied Mathematics,* in press (DOI:10.1016/j.cam.2006.04.010).

[16] M. N. Kashid, D. W. Agar, and S. Turek, *CFD modelling of mass transfer with and without chemical reaction in the liquid-liquid slug flow capillary microreactors*, Chemical Engineering Science, in press (DOI:10.1016/j.ces.2007.01.068).

[17] S. Komori, K. Nagata, T. Kanzaki and Y. Murakami, *Measurements of Mass Flux in a Turbulent Liquid Flow with a Chemical Reaction,* AIChE Journal **39**(10), 1993, pp.1611-1620.

[18] D. Kuzmin and M. Möller, *Algebraic Flux Correction I. Scalar Conservation Laws,* In: D. Kuzmin, R. Löhner and S. Turek (eds.) *Flux-Corrected Transport: Principles, Algorithms, and Applications,* 2005, Springer, pp.155-206.

[19] D. Kuzmin and M. Möller *Algebraic Flux Correction II. Compressible Euler equations.,* In: D. Kuzmin, R. Löhner and S. Turek (eds.) *Flux-Corrected Transport: Principles, Algorithms, and Applications*, 2005, Springer, pp.207-250.

[20] D. Kuzmin and O. Mierka, *On the implementation of the $k-\varepsilon$ turbulence model in incompressible flow solvers based on a finite element discretization,* Proceedings of the International Conference of Boundary and Interior Layers, Göttingen, Germany, 2006.

[21] D. Kuzmin and S. Turek, *Finite element discretization tools for gas-liquid flows,* In: M. Sommerfeld (ed.), Bubbly Flows: Analysis, Modelling and Calculation, Springer, 2004, pp.191-201.

[22] D. Kuzmin and S. Turek, *Numerical simulation of turbulent bubbly flows,* Technical report **254**, University of Dortmund, 2004. In: Proceedings of the Third International Symposium on Two-Phase Flow Modeling and Experimentation, Pisa, Italy, 2004.

[23] D. Kuzmin and S. Turek *Multidimensional FEM-TVD paradigm for convection-dominated flows, Technical report* **253**, University of Dortmund. In: *Proceedings of the IV European Congress on Computational Methods in Applied Sciences and Engineering*, 2004, Volume II, ISBN 951-39-1869-6.

[24] B. Launder and D. Spalding, *The numerical computation of turbulent flows,* Computer Methods in Applied Mechanics and Engineering, **3**(2), 1974, pp.269-289.

[25] A. J. Lew, G. C. Buscaglia and P. M. Carrica, *A Note on the Numerical Treatment of the k-epsilon Turbulence Model,* International Journal of Computational Fluid Dynamics, **14**, 2001, pp.201-209.

[26] J. Jie and Y. Renardy, *Numerical study of flows of two immiscible liquids at low Reynolds number,* Society for Industrial and applied Mathematics Review, **42**(3), 2000, pp.417-439.

[27] Y. S. Matros, *Catalytic Processes Under Unsteady-State Conditions,* Studies of surface Science and catalysis, Elsevier Science Ltd, 1989.

[28] O. Mierka, *CFD modelling of chemical reactions in turbulent liquid flows*, Ph.D. Thesis, Bratislava, Slovak Technical University, 2005.

[29] K. Nalpantidis, Untersuchung der heterogen/homogen Zersetzung von N_2O in einem periodisch betriebenen Festbettreaktor, Diploma thesis, University of Dortmund, 2003.

[30] K. Nalpantidis, F. Platte, D. W. Agar and S. Turek, *Elucidation of hybrid N_2O decomposition using axially structured catalyst in reverse flow reactor,* Chemical Engineering Science, **61**(10), 2006, pp.3176-3185.

[31] S. Osher and J. A. Sethian, *Fronts propagating with curvature-dependent speed: Algorithms based on Hamilton-Jacobi formulations,* Journal of Computational Physics, **79**(1), 1988, pp.12-49, (DOI: 10.1016/0021-9991(88)90002-2).

[32] F. Platte, D. Kuzmin, Ch. Fredebeul and S. Turek, *Novel simulation approaches for cyclic steady–state fixed–bed processes exhibiting sharp fronts and shocks,* International Series of Numerical Mathematics, **151**, 2005, pp.207-223, In: M. G. de Bruin, D. H. Mache & J. Szabados (eds.), *Trends and Applications in Constructive Approximation,* Birkhäuser Verlag Basel/Switzerland.

[33] K. Tsai, P. A. Gillis, S. Sen and R. O. Fox, *A Finite-Mode PDF Model for Turbulent Reacting Flows,* Journal of Fluids Engineering, **124**(1), 2002, pp.102-107.

[34] S. Turek, *Efficient Solvers for Incompressible Flow Problems: An Algorithmic and Computational Approach*, LNCSE **6**, Springer, 1999.

[35] S. Turek and D. Kuzmin, *Algebraic Flux Correction III. Incompressible Flow Problems,* In: D. Kuzmin, R. Löhner and S. Turek (eds.) *Flux-Corrected Transport: Principles, Algorithms, and Applications*, 2005, Springer, pp.251-296.

[36] D. Vortmeyer and R. J. Schäfer, *Equivalence of one and two -phase models for heat transfer in packed beds: one dimensional theory,* Chemical Engineering Science, **29**(2), 1974, pp.485-491.

[37] Ch. Yang and Z.-S. Mao, *Numerical simulation of interphase mass transfer with the levelset approach,* Chemical Engineering Science, **60**(10), 2005, pp.2643-2660.